

Direct Detection with Dark Mediators

David Curtin, Ze'ev Surujon

C. N. Yang Institute for Theoretical Physics, Stony Brook University, Stony Brook, NY 11794, U.S.A.

Yuhsin Tsai

Physics Department, University of California Davis, Davis, California 95616, U.S.A.

Abstract

We introduce *dark mediator Dark matter* (dmDM) where the dark and visible sectors are connected by at least one light mediator ϕ carrying the same dark charge that stabilizes DM. ϕ is coupled to the Standard Model via an operator $\bar{q}q\phi\phi^*/\Lambda$, and to dark matter via a Yukawa coupling $y_\chi\bar{\chi}\chi\phi$. Direct detection is realized as the $2 \rightarrow 3$ process $\chi N \rightarrow \bar{\chi} N \phi$ at tree-level for $m_\phi \lesssim 10$ keV and small Yukawa coupling, or alternatively as a loop-induced $2 \rightarrow 2$ process $\chi N \rightarrow \chi N$. We explore the direct-detection consequences of this scenario and find that a heavy $\mathcal{O}(100 \text{ GeV})$ dmDM candidate fakes different $\mathcal{O}(10 \text{ GeV})$ standard WIMPs in different experiments. Large portions of the dmDM parameter space are detectable above the irreducible neutrino background and not yet excluded by any bounds. Interestingly, for the m_ϕ range leading to novel direct detection phenomenology, dmDM is also a form of Self-Interacting Dark Matter (SIDM), which resolves inconsistencies between dwarf galaxy observations and numerical simulations.

1. Introduction

In this letter, we present *Dark Mediator Dark Matter* (dmDM) to address two important gaps in the DM literature: exploring mediators with dark charge, and non-standard interaction topologies for scattering off nuclei. Additional details and constraints will be explored in a companion paper [1].

The existence of dark matter is firmly established by many astrophysical and cosmological observations [2], but its mass and coupling to the Standard Model (SM) particles are still unknown. Weakly Interacting Massive Particles (WIMPs) are the most popular DM candidates since they arise in many theories beyond the SM, including supersymmetry, and may naturally give the correct relic abundance [3]. However, improved experimental constraints – from collider searches, indirect detection and direct detection [4, 5, 6, 7, 8, 9, 10, 11] – begin to set tight limits (with some conflicting signal hints) on the standard WIMP scenario with a contact interaction to quarks. This makes it necessary to look for a more complete set of DM models which are theoretically motivated while giving unique experimental signatures.

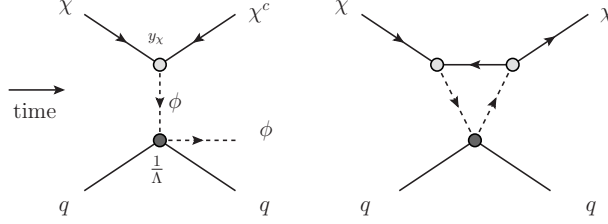


Figure 1: The quark-level Feynman diagrams responsible for DM-nucleus scattering in *Dark Mediator Dark Matter* (dmDM). Left: the $2 \rightarrow 3$ process at tree-level. Right: the loop-induced $2 \rightarrow 2$ process. The arrows indicate flow of dark charge.

2. Dark Mediator Dark Matter

Given its apparently long lifetime, most models of DM include some symmetry under which the DM candidate is charged to make it stable. An interesting possibility is that not only the DM candidate, but also the mediator connecting it to the visible sector is charged under this dark symmetry. Such a ‘dark mediator’ ϕ could only couple to the SM fields in pairs.

As a simple example, consider real or complex SM singlet scalars ϕ_i coupled to quarks, along with Yukawa couplings to a Dirac fermion DM candidate χ . The terms in the effective Lagrangian relevant for direct detection are

$$\mathcal{L}_{\text{DM}} \supset \sum_{i,j}^{n_\phi} \frac{1}{\Lambda_{ij}} \bar{q} q \phi_i \phi_j^* + \sum_i^{n_\phi} (y_\chi^{\phi_i} \bar{\chi} \chi \phi_i + h.c.) + \dots \quad (1)$$

where \dots stands for ϕ, χ mass terms, as well as the rest of the dark sector, which may be more complicated than this minimal setup. This interaction structure can be enforced by a \mathbb{Z}_4 symmetry. To emphasize the new features of this model for direct detection, we focus on the minimal case with a single mediator $n_\phi = 1$ (omitting the i -index). However, the actual number of dark mediators is important for interpreting indirect constraints [1].

The leading order process for DM-nucleus scattering is $\chi N \rightarrow \bar{\chi} N \phi$ if $m_\phi \lesssim \mathcal{O}(10 \text{ keV})$. However, an elastic scattering $\chi N \rightarrow \chi N$ is always present at loop-level since it satisfies all possible symmetries, see Fig. 1. Which of the two possibilities dominates direct detection depends on the size of the Yukawa couplings $y_\chi^{\phi_i}$ as well as the dark mediator masses.

Previous modifications to WIMP-nucleon scattering kinematics include the introduction of a mass splitting [12, 13, 14]; considering matrix elements $|\mathcal{M}|^2$ with additional velocity- or momentum transfer suppressions (for a complete list see e.g. [15]), especially at low DM masses close to a GeV [16]; light scalar or ‘dark photon’ mediators (see e.g. [17] which give large enhancements at low nuclear recoil); various forms of composite dark matter [18, 19, 20, 21, 22] which may introduce additional form factors; DM-nucleus scattering with intermediate bound states [23] which enhances scattering in a narrow range of DM velocities; and induced nucleon decay in Asymmetric Dark Matter models [24]. Notably missing from this list are

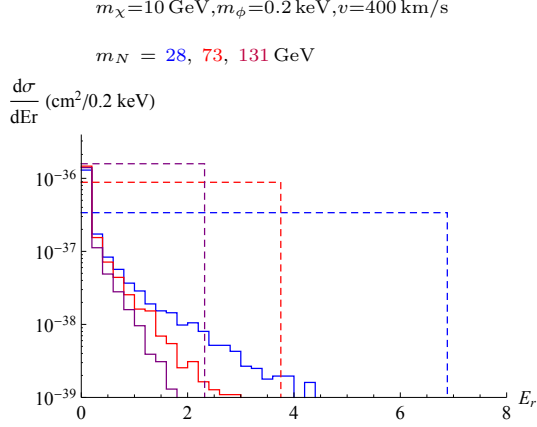


Figure 2: Nuclear recoil spectra of dmDM (without nuclear/nucleus form factors and coherent scattering enhancement) for $y_\chi = 1, \Lambda = 1 \text{ TeV}$ in a Silicon, Germanium and Xenon target. The dashed lines are spectra of standard WIMP scattering (via operator $\bar{q}q\bar{\chi}\chi/\tilde{\Lambda}^2$, with $\tilde{\Lambda} = 7 \text{ TeV}$) shown for comparison. dmDM spectra computed with **MadGraph5** [26] and **FeynRules1.4** [27].

alternative process topologies for DM-nucleus scattering. This omission is remedied by the dmDM scenario.

dmDM is uniquely favored to produce a detectable $2 \rightarrow 3$ scattering signal at direct detection experiments. This is because it contains two important ingredients: (1) a light mediator with non-derivative couplings to enhance the cross section, compensating for the large suppression of emitting a relativistic particle in a non-relativistic scattering process, and (2) a scalar as opposed to a vector mediator, allowing it to carry dark charge (without a derivative coupling). This imposes selection rules which make the $2 \rightarrow 2$ process subleading in y_χ . These ingredients are difficult to consistently implement in other model constructions without violating constraints on light force carriers.

The effect of strong differences between proton and neutron coupling to DM have been explored by [25]. To concentrate on the kinematics we shall therefore assume the operator $\bar{q}q\phi\phi^*/\Lambda$ is flavor-blind in the quark mass basis. Above the electroweak symmetry breaking scale this operator is realized as $\bar{Q}_L H q_R \phi\phi^*/M^2$. It can be generated by integrating out heavy vector-like quarks which couple to the SM and ϕ [1], giving $1/\Lambda = y_Q^2 y_h v/M_Q^2$. This UV completion allows for large direct detection cross sections without being in conflict with collider bounds, but may be still probed at the 14 TeV LHC.

3. Nuclear Recoil Spectrum

We start by examining the novel $2 \rightarrow 3$ regime of dmDM. The DM-nucleus collision is inelastic, not by introducing a new mass scale like a splitting, but by virtue of the process topology. The nuclear recoil spectrum is different compared to previously explored scenarios. This is illustrated in Fig. 2, where we

compare nuclear recoil spectra of standard WIMPs to dmDM for fixed velocity and different nucleus mass, *before* convolving with various form factors and the ambient DM speed distribution. The observable dmDM differential cross section is independent of m_ϕ for $m_\phi \lesssim \text{keV}$ and can be well described by the function

$$\frac{d\sigma_{2\rightarrow 3}}{dE_r} \simeq \frac{\mathcal{C}}{E_r} \left(1 - \sqrt{\frac{E_r}{E_r^{\max}}}\right)^2, \quad (2)$$

where $\mathcal{C} = 1.3 \times 10^{-42} (\text{TeV}/\Lambda)^2 \text{ cm}^2$ and $E_r^{\max} = \frac{2\mu_{\chi N}^2}{m_N} v^2$, same as the WIMP case for a given DM velocity. (We emphasize that this is a phenomenological description, the actual spectra were produced in MadGraph, see Section 5.) The first factor comes from the light mediator propagator $(2m_N E_r)^{-2}$ as well the integrated phase space of the escaping ϕ . The cross section suppression (second factor) is more pronounced as the DM becomes lighter or slower, and as the nucleus becomes heavier, both of which reduces E_r^{\max} . This is because massless ϕ emission carries away a more significant fraction of the total collision energy if the heavy particle momenta are smaller. The maximum kinematically allowed nuclear recoil is then less likely.

When $n_\phi = 1$, the $2 \rightarrow 2$ process will dominate direct detection for Yukawa coupling y_χ above some threshold, or if $m_\phi \gtrsim 10 \text{ keV}$. For the purpose of calculating the matrix element, the loop diagram in Fig. 1 (right) is equivalent to the operator

$$\frac{y_\chi^2}{2\pi^2} \frac{1}{\Lambda q} (\bar{\chi} \chi \bar{N} N), \quad (3)$$

where $q = \sqrt{2m_N E_r}$ is the momentum transfer in the scattering. Effectively, this is identical to a standard WIMP with a $\bar{\chi}\chi\bar{N}N$ contact operator, but with an additional $1/E_r$ suppression in the cross section. This gives a similar phenomenology as a light mediator being exchanged at tree-level with derivative coupling.

Note that the relative importance of these two scattering processes is highly model dependent. For example, if $n_\phi = 2$ the dominant scalar-DM coupling could be $\bar{q}q\phi_1\phi_2^*/\Lambda_{12}$. In that case, the $2 \rightarrow 2$ operator above is $\propto y_\chi^{\phi_1} y_\chi^{\phi_2}$ and can be suppressed without reducing the $2 \rightarrow 3$ rate by taking $y_\chi^{\phi_2} \gg y_\chi^{\phi_1}$. The scattering behavior of both the $2 \rightarrow 3$ and $2 \rightarrow 2$ regimes necessitates a re-interpretation of all DM direct detection bounds. We will do this below.

4. Indirect Constraints

Direct detection experiments probe the ratio y_χ/Λ and y_χ^2/Λ for $2 \rightarrow 3$ and $2 \rightarrow 2$ scattering respectively. However, indirect constraints on dmDM from cosmology, stellar astrophysics and collider experiments are sensitive to the Yukawa coupling and Λ separately. In [1] we conduct an extensive study of these bounds, including the first systematic exploration of constraints on the $\bar{q}q\phi\phi^*/\Lambda$ operator with light scalars ϕ . Since these constraints (in particular, Eqns. 4 and 5 below) provide important context for our results on direct detection, we summarize the two most important results here. For details we refer the reader to [1].

The scalar mediator(s) of dmDM are most stringently constrained from stellar astrophysics and cosmology:

- Avoiding overclosure requires $m_\phi \lesssim \text{eV}$ [28], so we take the heaviest stable ϕ to be essentially massless, making it a very subdominant dark matter component. This also satisfies structure formation, computed for light sterile neutrinos in [29]. Measurements by the Planck satellite [2] restrict the number of light degrees of freedom during Big Bang Nucleosynthesis, enforcing the bound $n_\phi \leq 2$ for real scalars.
- The coupling of ϕ to the SM is most constrained from stellar astrophysics. For $n_\phi = 1$, observational data on neutron star cooling essentially rules out any directly detectable dmDM model [1]. However, this bound is easily relaxed for $n_\phi = 2$ if $m_{\phi_1} \lesssim \text{eV}$, $m_{\phi_2} \sim \text{MeV}$, with a cosmologically unstable ϕ_2 . The dominant interaction to the SM is assumed to be $\bar{q}q\phi_1\phi_2^*/\Lambda$. In that case, ϕ_2 emission in the neutron star is Boltzmann suppressed due to its core temperature of $T \lesssim 100 \text{ keV}$, and ϕ_1 emission proceeds via a loop process. The bound on Λ is then weakened to

$$\Lambda \gtrsim 10 \text{ TeV}. \quad (4)$$

- In Supernovae, emission of light invisible particles can truncate the neutrino burst [30]. However, if these particles interact with the stellar medium more strongly than neutrinos they are trapped and do not leak away energy from the explosion. The temperature of supernovae $T \sim 10 \text{ MeV}$ is large enough to produce ϕ_1, ϕ_2 at tree-level in the above $n_\phi = 2$ scenario, and the scattering cross section with nuclei is much larger than for neutrinos if $\Lambda \lesssim 10^6 \text{ TeV}$. Therefore this setup is compatible with supernovae constraints.
- The LHC can set constraints on heavy dark vector quarks in a possible UV completion of dmDM. The CMS 20 fb^{-1} di-jet + MET search [31] search sets a lower bound on the heavy quark to be 1.5 TeV .

The physics of direct detection for this $n_\phi = 2$ setup is identical to the minimal $n_\phi = 1$ model. This is because the typical momentum transfer is $\mathcal{O}(10 \text{ MeV})$, making the intermediate ϕ_2 mediator massless for the purposes of direct detection. We are therefore justified in examining the direct detection phenomenology of the $n_\phi = 1$ model in detail, applying the Λ bound Eqn. 4 and with the understanding that the full realization of dmDM requires a slightly non-minimal spectrum.

The dark matter yukawa coupling is constrained from observations on large scale structure and (under certain assumptions) from cosmology:

- Dark matter self-interaction bounds from bullet cluster observations constrain the DM Yukawa coupling to be $y_\chi \lesssim 0.13(m_\chi/\text{GeV})^{3/4}$ [32].
- A thermal relic χ with $\Omega_\chi = \Omega_{\text{CDM}}$ requires

$$y_\chi = y_\chi^{\text{relic}}(m_\chi) \approx 0.0027 \left(\frac{m_\chi}{\text{GeV}} \right)^{1/2} \quad (5)$$

if there is no significant ϕ^3 term. This also satisfies the above self-interaction bounds.

Interestingly, the range of $m_\phi \sim \text{eV}$ to MeV that is relevant for its novel direct detection signal also makes dmDM a realization of Self-Interacting DM (SIDM) [33, 34, 35, 36, 37, 38, 39, 40]. A Yukawa interaction consistent with χ being a thermal relic can then help resolve the “core/cusp” and “too-big-to-fail” inconsistencies between dwarf galaxy observations and many-body simulations [1, 40].

5. Direct Detection

We compute dmDM nuclear recoil spectra at direct detection experiments by simulating the parton-level process in `MadGraph5` [26], and derive the event rates according to

$$\frac{dR}{dE_r} = N_T \frac{\rho_\chi}{m_\chi} \int dv v f(v) \frac{d\sigma_N}{dE_r}, \quad (6)$$

where $f(v)$ is the local DM speed distribution (approximate Maxwell-Boltzmann with $v_0 \approx 220 \text{ km/s}$ and a $v_{esc} \approx 544 \text{ km/s}$ cutoff, boosted into the earth frame $v_e \approx 233$ [41]), while $\rho_\chi \approx 0.3 \text{ GeV cm}^{-3}$ is the local DM density [42], and N_T is the target number density per kg. $d\sigma_N/dE_r$ includes the usual Helm nuclear form factor [43, 44], the A^2 coherent scattering enhancement as well as the quark-nucleon form factor for scalar interactions (see [45] for a review). We validated our Monte Carlo pipeline by reproducing analytically known $2 \rightarrow 2$ results.

Fig. 3 shows some nuclear recoil spectra for a Silicon and Xenon target. (We henceforth assume an effectively massless ϕ .) dmDM is compared to standard WIMPs (velocity- and recoil-independent contact-interaction) for different DM masses. An important feature of our model is apparent: a $\sim 50 \text{ GeV}$ dmDM candidate looks like a $\sim 10 \text{ GeV}$ (20 GeV) WIMP when scattering off Silicon (Xenon). Moreover, the shape of $d\sigma_N/dE_r$ is insensitive to m_χ unless m_χ is much smaller than m_N (see Eq. 2). This makes it much more difficult to measure the DM mass using the shape of the spectrum. Signals at two detectors with different target materials are required.

We can make this observation more concrete by mapping dmDM parameters to WIMP parameters. This is possible because both sets of nuclear recoil spectra look roughly like falling exponentials. For each dmDM spectrum with a given mass there is a closely matching WIMP spectrum with some different (lower) mass. To find the $m_{2 \rightarrow 2}$ corresponding to each $m_{2 \rightarrow 3}$ we compare binned WIMP and dmDM distributions and minimize the total relative difference in each bin. The resulting mapping is shown in Fig. 4 (left). Even very heavy dmDM candidates mimic light WIMPs of different masses at different experiments. A corresponding cross section remapping (right) shows that experiments with heavier nuclei are more sensitive to dmDM due to the inelastic nature of the collision.

Fig. 4 defines an experiment-dependent parameter map that we can use to map each collaboration’s WIMP bounds onto the dmDM model if $2 \rightarrow 3$ scattering dominates¹. The resulting direct detection bounds

¹We have confirmed the validity of this approach with full maximum likelihood fits [47].

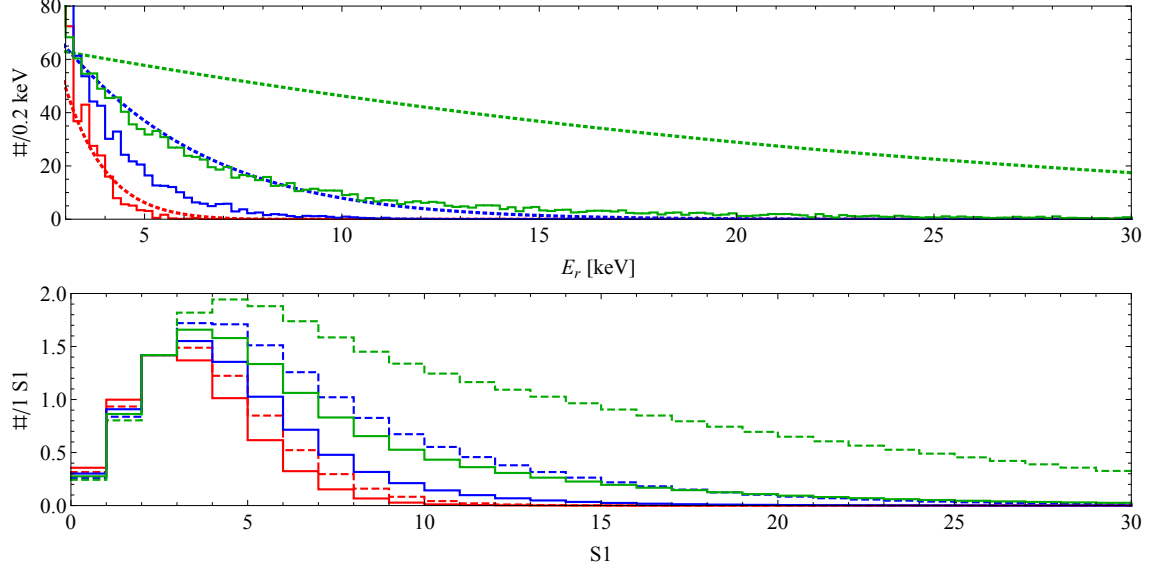


Figure 3: **Top:** Nuclear recoil spectra at CDMS II Silicon ($m_N = 28$ GeV) with 140.2 kg-days exposure for dmDM (solid) and WIMP DM (dotted) of mass 5 (red), 10 (blue) and 50 (green) GeV. Experimental efficiencies are not included, and the recoil spectrum is shown only for $E_r > 3$ keV because the dmDM spectrum is so sharply peaked at the origin that no other features would be visible if it were included. The shown WIMP-nucleon cross sections for (5, 10, 50) GeV are $(4, 2, 6) \times 10^{-40}$ cm², while the dmDM parameters are $y_\chi = 0.02$, $\Lambda = (29, 91, 91)$ TeV and $m_\phi < \text{keV}$. **Bottom:** S1 spectra at LUX ($m_N = 131$ GeV) with 10065.4 kg-days exposure for dmDM (solid) and WIMP DM (dotted) of mass 10 (red), 20 (blue) and 50 (green) GeV. The 14% S1 light gathering efficiency is included but selection cuts are not. No DM signal below $E_r = 3$ keV is included due to limitations of the measured \mathcal{L}_{eff} , in accordance with the collaboration's analysis. The shown WIMP-nucleon cross sections for (10, 20, 50) GeV are $(18.5, 3.6, 4.9) \times 10^{-45}$ cm², while the dmDM parameters are $y_\chi = 0.02$ and $\Lambda = (1900, 9700, 13000)$ TeV and $m_\phi < \text{keV}$.

are shown in Fig. 5 (left). We include the irreducible neutrino background [46] at the LUX experiment, which serves as an approximate lower border of the observable dmDM parameter space. An identical procedure can be used in the $2 \rightarrow 2$ dominant regime of dmDM. The translation map has similar qualitative features to the previous case since $d\sigma/dE_r \sim E_r^{-1}$, except the faked WIMP signal corresponds to somewhat higher mass. The resulting direct detection bounds are shown in Fig. 5 (right).

The probability for any one $2 \rightarrow 2$ nuclear recoil event to lie above experimental detection threshold is much larger than for a $2 \rightarrow 3$ event, due to the less severe recoil suppression. For $n_\phi = 1$, this means the former will dominate direct detection unless $m_\phi \lesssim \text{keV}$ and the Yukawa coupling is very small, $y_\chi \lesssim 10^{-3} < y_\chi^{\text{relic}}$. However, as discussed in Section 4, the neutron star cooling constraint requires at least $n_\phi = 2$. The $2 \rightarrow 2$ process could then be arbitrarily suppressed, allowing $2 \rightarrow 3$ direct detection with a thermal relic χ .

For the $2 \rightarrow 3$ and $2 \rightarrow 2$ scattering regimes, direct detection probes y_χ/Λ and y_χ^2/Λ respectively. The neutron star cooling bound $\Lambda \gtrsim 10$ TeV and the bounds on dark matter Yukawa coupling y_χ can be combined to be shown in the direct detection planes of Fig. 5. The assumption of a thermal relic then

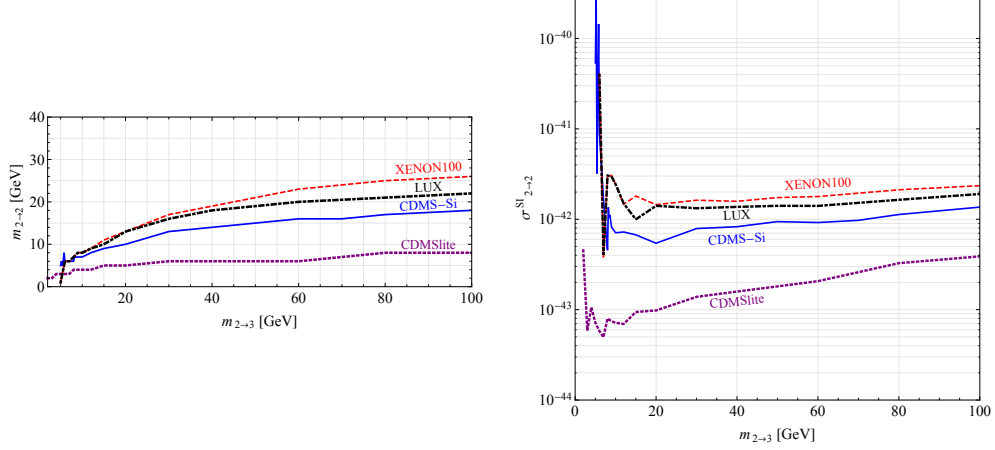


Figure 4: **Left:** For each dmDM mass $m_\chi = m_{2 \rightarrow 3}$ this plot shows the WIMP mass $m_\chi = m_{2 \rightarrow 2}$ which gives the same spectral shape at XENON100 ($S1 > 3$ with 6% light gathering efficiency, dashed red line), LUX ($S1 > 2$ with 14% light gathering efficiency, dash-dotted black line), CDMSII Silicon ($E_T > 7$ keV, solid blue line), and CDMSlite (Germanium, $E_T > 0.2$ keV, dotted purple line) before selection cuts. **Right:** The ‘observed’ WIMP-nucleon cross section for each dmDM mass $m_{2 \rightarrow 3}$, assuming the best-fit $m_{2 \rightarrow 2}$ from the left. The dmDM parameters are $y_\chi = 1, \Lambda = 45$ TeV.

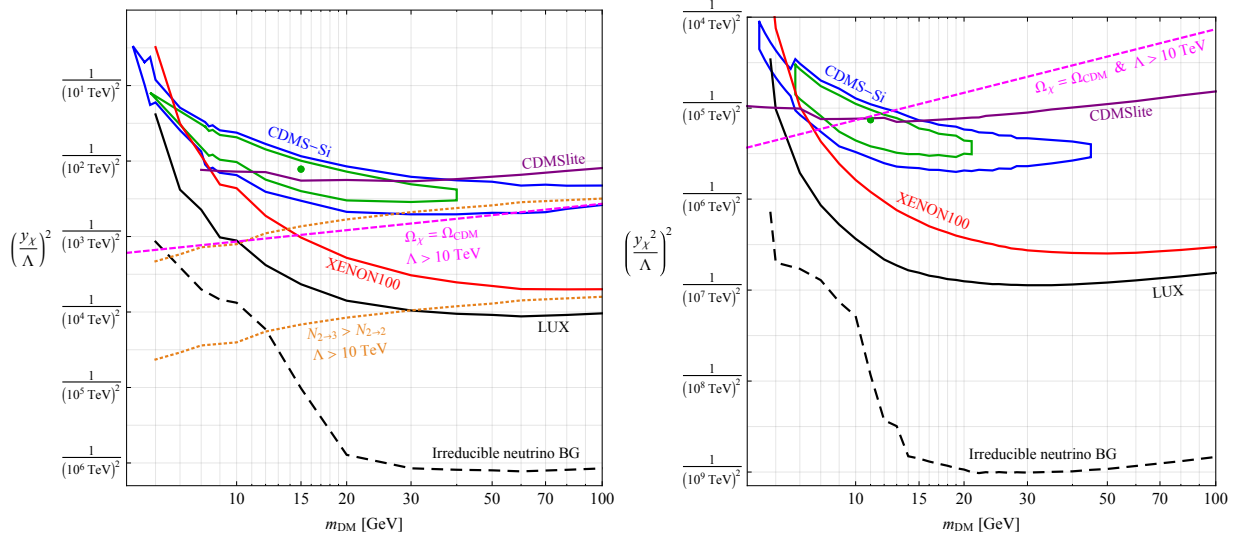


Figure 5: **Left:** Direct detection bounds on the $2 \rightarrow 3$ regime of dmDM. The vertical axis is proportional to $\sigma_{\chi N \rightarrow \bar{\chi} N \phi}$. *Solid lines:* 90% CL bounds by XENON100 (red), LUX (black) and CDMSlite (purple), as well as the best-fit regions by CDMS II Si (blue, green). The large-dashed black line indicates the irreducible neutrino background [46]. *Small-dashed magenta line:* Upper bound for $y_\chi = y_\chi^{\text{relic}}(m_\chi)$ and neutron star cooling bound $\Lambda < 10$ TeV. *Lower dotted orange line:* upper bound for $2 \rightarrow 3$ dominated direct detection and neutron star bound with all equal Yukawa couplings. This line can be arbitrarily moved, as discussed below Eq. 3. The *upper dotted orange line* is for $y_\chi^{\phi_1} = y_\chi^{\phi_2}/20$, in which case the vertical axis is understood to be $(y_\chi^{\phi_2}/\Lambda)^2$. **Right:** Direct detection bounds on the $2 \rightarrow 2$ regime of $n_\phi = 1$ dmDM, same labeling as the left plot. The vertical axis is proportional to $\sigma_{\chi N \rightarrow \bar{\chi} N}$, and is understood to be $(y_\chi^1 y_\chi^2/\Lambda)^2$ for the $n_\phi = 2$ model outlined in Section 4.

excludes the regions in Fig. 5 above the magenta dashed line, meaning these bounds supersede the liquid Xenon experiments for $m_\chi \lesssim 10$ GeV in the $2 \rightarrow 3$ dominant regime.

There are large discoverable regions of dmDM parameter space that are not excluded. Due to the nontrivial dependence of the dmDM recoil spectrum on the target- and dark-matter masses and velocity, signals at several experiments will be needed to differentiate standard WIMPs from our model, but dmDM offers the realistic prospect of TeV-scale heavy quark discoveries pointing the way towards a sensitivity target for direct detection.

6. Conclusion

Dark Mediator Dark Matter introduces the possibility that dark matter interacts with the standard model via a mediator which also carries dark charge. This “Double-Dark Portal” adds the phenomenon of additional particle emission to the menu of possible interactions with nuclei, serving as an existence proof that this scattering topology can be realized. Direct detection experiments are starting to probe interesting regions of parameter space compatible with a thermal relic and neutron star bounds. For observationally relevant parameters, dmDM also acts as an implementation of SIDM [33, 34, 35, 36, 37, 38, 39, 40], which can resolve various inconsistencies between many-body simulations and observations for dwarf galaxies. Even more than many other DM models, dmDM discovery is aided by lowering nuclear recoil thresholds. Further investigation is warranted and includes potential LHC signals, as well as possible leptophilic realizations of the model.

Acknowledgements — The authors would like to gratefully acknowledge the valuable contributions of Yue Zhao during an earlier stage of this collaboration. We thank Rouven Essig, Patrick Fox, Roni Harnik and Patrick Meade for valuable comments on draft versions of this letter. We are very grateful to Joseph Bramante, Rouven Essig, Greg Gabadadze, Jasper Hasenkamp, Matthew McCullough, Olivier Mattelaer, Matthew Reece, Philip Schuster, Natalia Toro, Sean Tulin, Neal Weiner, Itay Yavin and Hai-Bo Yu for valuable discussions. D.C. and Z.S. are supported in part by the National Science Foundation under Grant PHY-0969739. Y.T. is supported in part by the Department of Energy under Grant DE-FG02-91ER40674. The work of Y.T. was also supported in part by the National Science Foundation under Grant No. PHYS-1066293 and the hospitality of the Aspen Center for Physics

References

- [1] D. Curtin and Y. Tsai, arXiv:1405.1034 [hep-ph].
- [2] P. A. R. Ade *et al.* [Planck Collaboration], arXiv:1303.5076 [astro-ph.CO].

- [3] See, for example, G. Jungman, M. Kamionkowski and K. Griest, Phys. Rept. **267**, 195 (1996) [hep-ph/9506380]. G. Bertone and D. Merritt, Mod. Phys. Lett. A **20**, 1021 (2005) [astro-ph/0504422].
- [4] M. W. Goodman and E. Witten, Phys. Rev. D **31**, 3059 (1985).
- [5] D. S. Akerib *et al.* [LUX Collaboration], arXiv:1310.8214 [astro-ph.CO].
- [6] E. Aprile *et al.* [XENON100 Collaboration], Phys. Rev. Lett. **109**, 181301 (2012) [arXiv:1207.5988 [astro-ph.CO]].
- [7] R. Bernabei, P. Belli, S. d’Angelo, A. Di Marco, F. Montecchia, F. Cappella, A. d’Angelo and A. Incicchitti *et al.*, Int. J. Mod. Phys. A **28**, 1330022 (2013) [arXiv:1306.1411 [astro-ph.GA]].
- [8] C. E. Aalseth *et al.* [CoGeNT Collaboration], Phys. Rev. D **88**, 012002 (2013) [arXiv:1208.5737 [astro-ph.CO]].
- [9] G. Angloher, M. Bauer, I. Bavykina, A. Bento, C. Bucci, C. Ciemniak, G. Deuter and F. von Feilitzsch *et al.*, Eur. Phys. J. C **72**, 1971 (2012) [arXiv:1109.0702 [astro-ph.CO]].
- [10] R. Agnese *et al.* [CDMS Collaboration], [arXiv:1304.4279 [hep-ex]].
- [11] T. Cohen, M. Lisanti, A. Pierce and T. R. Slatyer, JCAP **1310**, 061 (2013) [arXiv:1307.4082 [hep-ph]]. J. Fan and M. Reece, JHEP **1310**, 124 (2013) [arXiv:1307.4400 [hep-ph]].
- [12] D. Tucker-Smith and N. Weiner, Phys. Rev. D **64**, 043502 (2001) [hep-ph/0101138].
- [13] P. W. Graham, R. Harnik, S. Rajendran and P. Saraswat, Phys. Rev. D **82**, 063512 (2010) [arXiv:1004.0937 [hep-ph]].
- [14] R. Essig, J. Kaplan, P. Schuster and N. Toro, [arXiv:1004.0691 [hep-ph]].
- [15] J. March-Russell, J. Unwin and S. M. West, JHEP **1208**, 029 (2012) [arXiv:1203.4854 [hep-ph]].
- [16] S. Chang, A. Pierce and N. Weiner, JCAP **1001**, 006 (2010) [arXiv:0908.3192 [hep-ph]].
- [17] R. Essig, J. A. Jaros, W. Wester, P. H. Adrian, S. Andreas, T. Averett, O. Baker and B. Batell *et al.*, arXiv:1311.0029 [hep-ph].
- [18] D. S. M. Alves, S. R. Behbahani, P. Schuster and J. G. Wacker, Phys. Lett. B **692**, 323 (2010) [arXiv:0903.3945 [hep-ph]].
- [19] G. D. Kribs, T. S. Roy, J. Terning and K. M. Zurek, Phys. Rev. D **81**, 095001 (2010) [arXiv:0909.2034 [hep-ph]].

- [20] M. Lisanti and J. G. Wacker, Phys. Rev. D **82**, 055023 (2010) [arXiv:0911.4483 [hep-ph]].
- [21] J. M. Cline, A. R. Frey and G. D. Moore, Phys. Rev. D **86**, 115013 (2012) [arXiv:1208.2685 [hep-ph]].
- [22] B. Feldstein, A. L. Fitzpatrick and E. Katz, JCAP **1001**, 020 (2010) [arXiv:0908.2991 [hep-ph]].
- [23] Y. Bai and P. J. Fox, JHEP **0911**, 052 (2009) [arXiv:0909.2900 [hep-ph]].
- [24] H. Davoudiasl, D. E. Morrissey, K. Sigurdson and S. Tulin, Phys. Rev. D **84**, 096008 (2011) [arXiv:1106.4320 [hep-ph]].
- [25] J. L. Feng, J. Kumar, D. Marfatia and D. Sanford, Phys. Lett. B **703**, 124 (2011) [arXiv:1102.4331 [hep-ph]].
- [26] J. Alwall, M. Herquet, F. Maltoni, O. Mattelaer and T. Stelzer, JHEP **1106**, 128 (2011) [arXiv:1106.0522 [hep-ph]].
- [27] S. Ask, N. D. Christensen, C. Duhr, C. Grojean, S. Hoeche, K. Matchev, O. Mattelaer and S. Mrenna *et al.*, arXiv:1209.0297 [hep-ph].
- [28] E. W. Kolb and M. S. Turner, Front. Phys. **69**, 1 (1990).
- [29] M. Wyman, D. H. Rudd, R. A. Vanderveld and W. Hu, arXiv:1307.7715 [astro-ph.CO].
- [30] G. G. Raffelt, Lect. Notes Phys. **741**, 51 (2008) [hep-ph/0611350].
- [31] CMS Collaboration [CMS Collaboration], CMS-PAS-SUS-13-012.
- [32] J. L. Feng, M. Kaplinghat, H. Tu and H. -B. Yu, JCAP **0907**, 004 (2009) [arXiv:0905.3039 [hep-ph]].
- [33] E. D. Carlson, M. E. Machacek and L. J. Hall, Astrophys. J. **398**, 43 (1992)
- [34] D. N. Spergel and P. J. Steinhardt, Phys. Rev. Lett. **84**, 3760 (2000) [astro-ph/9909386].
- [35] B. D. Wandelt, R. Dave, G. R. Farrar, P. C. McGuire, D. N. Spergel and P. J. Steinhardt, astro-ph/0006344.
- [36] A. Loeb and N. Weiner, Phys. Rev. Lett. **106**, 171302 (2011) [arXiv:1011.6374 [astro-ph.CO]].
- [37] M. Rocha, A. H. G. Peter, J. S. Bullock, M. Kaplinghat, S. Garrison-Kimmel, J. Onorbe and L. A. Moustakas, Mon. Not. Roy. Astron. Soc. **430**, 81 (2013) [arXiv:1208.3025 [astro-ph.CO]].
- [38] J. Zavala, M. Vogelsberger and M. G. Walker, Monthly Notices of the Royal Astronomical Society: Letters **431**, L20 (2013) [arXiv:1211.6426 [astro-ph.CO]].
- [39] M. VMedvedev, arXiv:1305.1307 [astro-ph.CO].

- [40] S. Tulin, H. -B. Yu and K. M. Zurek, Phys. Rev. D **87**, no. 11, 115007 (2013) [arXiv:1302.3898 [hep-ph]].
- [41] M. C. Smith, G. R. Ruchti, A. Helmi, R. F. G. Wyse, J. P. Fulbright, K. C. Freeman, J. F. Navarro and G. M. Seabroke *et al.*, Mon. Not. Roy. Astron. Soc. **379**, 755 (2007) [astro-ph/0611671].
- [42] J. Bovy and S. Tremaine, Astrophys. J. **756**, 89 (2012) [arXiv:1205.4033 [astro-ph.GA]].
- [43] J. Engel, Phys. Lett. B **264**, 114 (1991).
- [44] J. D. Lewin and P. F. Smith, Astropart. Phys. **6**, 87 (1996).
- [45] G. Belanger, F. Boudjema, A. Pukhov and A. Semenov, Comput. Phys. Commun. **180**, 747 (2009) [arXiv:0803.2360 [hep-ph]].
- [46] J. Billard, L. Strigari and E. Figueroa-Feliciano, arXiv:1307.5458 [hep-ph].
- [47] R. J. Barlow, Nucl. Instrum. Meth. A **297**, 496 (1990).